

# INFERENCE, FAST AND SLOW: REINTERPRETING VAES FOR OOD DETECTION

**Anonymous authors**

Paper under double-blind review

## ABSTRACT

Although likelihood-based methods are theoretically appealing, deep generative models (DGMs) often produce unreliable likelihood estimates in practice, particularly for out-of-distribution (OOD) detection. We reinterpret variational autoencoders (VAEs) through the lens of *fast and slow weights*. Our approach is guided by the proposed *Likelihood Path (LPath) Principle*, which extends the classical likelihood principle. A critical decision in our method is the selection of statistics for classical density estimation algorithms. The sweet spot should contain just enough information that’s sufficient for OOD detection but not too much to suffer from the curse of dimensionality. Our LPath principle achieves this by selecting the sufficient statistics that form the "path" toward the likelihood. We demonstrate that this likelihood path leads to SOTA OOD detection performance, even when the likelihood itself is unreliable.

## 1 INTRODUCTION

Independent and identically distributed (IID) samples during training and testing are key to much of machine learning’s (ML) success. However, as ML systems are deployed in the real world, encountering out-of-distribution (OOD) data is inevitable and poses significant safety risks. This is particularly challenging in the most general setting where labels are absent, and test input arrives in a streaming fashion. The objective of general *unsupervised OOD detection* is to develop a scalar score function, trained on  $P_{ID}$  (in-distribution (ID) samples), that assigns higher scores to data from  $P_{OOD}$  (out-of-distribution samples) than to data from  $P_{ID}$ .

Naïve approaches, such as using  $p_{\theta}(\mathbf{x})$ , the likelihood of deep generative models (DGMs), are attractive in theory but have proven ineffective due to unreliable likelihood estimates, often assigning high likelihood to OOD data (Nalisnick et al., 2018). Furthermore, even with perfect density estimation, likelihood alone is insufficient to detect OOD data (Le Lan & Dinh, 2021; Zhang et al., 2021) when the ID and OOD distributions overlap. Compounding this, recent theoretical works (Behrmann et al., 2021; Dai et al.) show that perfect density estimation may be infeasible for many DGMs.

Research Question (RQ) 1: Can we achieve state-of-the-art (SOTA) unsupervised OOD detection without relying on accurate likelihood estimation?

We take a step towards answering this question by developing a *principled* method for unsupervised OOD detection. Our algorithm is inspired by a reinterpretation of Variational Autoencoders (VAEs) from the *fast and slow weights perspective*, originally proposed in the context of adaptive neural networks and meta-learning (Hinton & Plaut, 1987; Munkhdalai & Trischler, 2018; Ba et al., 2016). Our algorithm has two stages. In the first stage (**neural feature extraction**), we train VAEs and extract key statistics contributing to the likelihood function. In the second stage (**classical density estimation**), these statistics are used as training data to fit a classical statistical density estimation algorithm (COPOD (Li et al., 2020) or MD (Lee et al., 2018; Maciejewski et al., 2022)) for OOD detection.

The key design decision in our algorithm is the choice of statistics, which leads to our second research question:

RQ 2: How do we select key statistics for the classical density estimation algorithm?

The desired statistics should strike a balance: including too many activations leads to the curse of dimensionality, while including too few fails to capture enough information. Our approach is to select the *minimal sufficient* statistics of the main components on the computational graph leading to the likelihood function. These anchoring statistics define the computational path of the likelihood function, which we term the *Likelihood Path (LPath) Principle*.

Under imperfect likelihood estimation, there is more information in the computational path leading to the marginal likelihood function  $p_\theta(\mathbf{x})$  relative to  $p_\theta(\mathbf{x})$  alone. Information can be optimally extracted by the *minimal sufficient statistics* of the individual components of the factorization of the likelihood function.

Although the LPath principle has independent interest in representation learning and can be applied to other DGMs, this work focuses on a thorough case study of applying the LPath principle to the OOD detection problem using Gaussian VAEs. We take the sufficient statistics of the VAE encoder and decoder as key statistics for our two-stage algorithm, achieving SOTA performance on common benchmarks (Table 1). Compared to other SOTA methods, we used a much smaller model (DC-VAEs from Xiao et al. (2020)’s architecture) with a parameter count of **3M**, compared to **44M** for Glow in DoSE (Morningstar et al., 2021) and **46M** for the diffusion model (Liu et al., 2023). We believe this “achieving more with less” phenomenon demonstrates our method’s potential.

To summarize, our main contributions are:

**Empirical contribution:** We achieved SOTA unsupervised OOD detection performance on common benchmarks (Table 1) using a much smaller model compared to other SOTA methods, addressing RQ1.

**Methodological contribution:** We proposed the LPath Principle, which generalizes the classical likelihood principle<sup>1</sup> for instance-dependent inference (e.g., OOD detection) under imperfect density estimation, addressing RQ2.

## 2 INFERENCE, FAST AND SLOW

In this section, we reinterpret VAEs from the perspective of fast and slow weights. We begin by clearly distinguishing between likelihood evaluation and parameter inference procedures, as this distinction will be important throughout the paper.

**Inferential Procedure** Given training data  $\mathbf{X}_{\text{Train}} = \{\mathbf{x}_i\}_{i=1}^N$  and a density model  $p_{\text{Model}} = p_\psi$  parameterized by  $\psi$ , we train  $p_\psi$  on  $\mathbf{X}_{\text{Train}}$  to obtain  $p_{\psi_{\text{trained}}}$ . This is an *inferential procedure*, transferring knowledge from  $\mathbf{X}_{\text{Train}}$  to the trained parameters  $\psi_{\text{trained}}$ :

$$(\mathbf{X}_{\text{Train}}, p_\psi) \longrightarrow \psi_{\text{trained}} \in \Psi, \quad (1)$$

where  $\Psi$  is the parameter space.

**Evaluation Procedure** Suppose we have a new sample  $\mathbf{x}$ ; we can compute the likelihood of  $\mathbf{x}$  under the trained model  $p_\psi$ . This is an *evaluation procedure*, assessing  $\mathbf{x}$  using the knowledge gained from training:

$$(\mathbf{x}, \psi_{\text{trained}}) \longrightarrow p_{\psi_{\text{trained}}}(\mathbf{x}) \in \mathbb{R}. \quad (2)$$

This typically occurs during test-time likelihood evaluation, after training is completed. However, direct application of this likelihood evaluation can assign higher likelihoods to OOD data than to ID data (Nalisnick et al., 2018).

While the evaluation procedure returns a scalar, the inferential procedure outputs a density model or parameters that characterize a model.

### 2.1 VAEs BACKGROUND

We use  $P$  to denote distributions and  $p$  as their associated densities. Variational Autoencoders (VAEs) (Kingma & Welling, 2013) are a distinct member of the family of deep generative models

<sup>1</sup>The marginal likelihood  $p_\theta(\mathbf{x})$  is a special case, as it only uses the endpoint in the likelihood path.

(DGMs), where the likelihood is computed by marginalizing the following joint model likelihood  $p_\theta(\mathbf{x}, \mathbf{z})$ , parameterized by  $\theta$ :  $p_\theta(\mathbf{x}) = \int_{\mathbf{z} \sim P(\mathbf{z})} p_\theta(\mathbf{x}, \mathbf{z}) d\mathbf{z}$ .

Here,  $p_\theta(\mathbf{x})$  is called the marginal likelihood and is treated as a function of  $\theta$ . VAEs are classified as *latent variable models* (Kingma et al., 2019), where latent variables  $\mathbf{z}$  represent unobserved random variables modeled as the source of the data-generating process. The marginal likelihood can be expressed as:

$$p_\theta(\mathbf{x}) = \int_{\mathbf{z} \sim P(\mathbf{z})} p_\theta(\mathbf{x}, \mathbf{z}) d\mathbf{z} = \int_{\mathbf{z} \sim P(\mathbf{z})} p_\theta(\mathbf{x} | \mathbf{z}) p(\mathbf{z}) d\mathbf{z}. \quad (3)$$

When both the prior  $P(\mathbf{z})$  and the conditional distribution  $P_\theta(\mathbf{x} | \mathbf{z})$  are Gaussian, the marginal likelihood  $p_\theta(\mathbf{x})$  can be thought of as an infinite Gaussian mixture model, making it highly expressive. However, in high-dimensional settings (e.g., images), directly estimating  $\log p_\theta(\mathbf{x}) = \log [p_\theta(\mathbf{x} | \mathbf{z}) p(\mathbf{z})] \approx \log(\frac{1}{K} \sum_{k=1}^K [p_\theta(\mathbf{x} | \mathbf{z}_k) p(\mathbf{z}_k)])$  with finite samples becomes computationally inefficient. VAEs introduce an efficient sampling method via an encoder  $q_\phi(\mathbf{z} | \mathbf{x})$  that serves as an importance-weighted sampler, making computation much more tractable. This is formalized as:

$$p_\theta(\mathbf{x}) = \int_{\mathbf{z} \sim P(\mathbf{z})} p_\theta(\mathbf{x} | \mathbf{z}) p(\mathbf{z}) d\mathbf{z} = \int_{\mathbf{z} \sim q_\phi(\mathbf{z} | \mathbf{x})} \frac{p_\theta(\mathbf{x} | \mathbf{z}) p(\mathbf{z})}{q_\phi(\mathbf{z} | \mathbf{x})} d\mathbf{z}, \quad (4)$$

with a one-sample approximation:

$$\log p_\theta(\mathbf{x}) \approx \log \left[ \frac{p_\theta(\mathbf{x} | \mathbf{z}) p(\mathbf{z})}{q_\phi(\mathbf{z} | \mathbf{x})} \right]. \quad (5)$$

For out-of-distribution (OOD) detection, we utilize the test-time latent variable inference of VAEs, so we omit the training dynamics here. For more details on VAEs, see Doersch (2016); Kingma et al. (2019).

**Gaussian VAEs** We next provide concrete examples of conditional distributions parameterized by encoder  $q_\phi(\mathbf{z} | \mathbf{x})$  and decoder  $p_\theta(\mathbf{x} | \mathbf{z})$  neural networks, as well as the prior. We choose Gaussian VAEs for illustration because they are widely used and have very simple *minimal sufficient statistics*.

In our setup, the prior distribution is a standard Gaussian distribution:

$$p(\mathbf{z}) = \mathcal{N}(\mathbf{z} | \boldsymbol{\mu} = \mathbf{0}, \boldsymbol{\Sigma} = \mathbf{I}). \quad (6)$$

The encoder is a Gaussian distribution parameterized by an encoder neural network with parameters  $\phi$ :

$$(\boldsymbol{\mu}_z(\mathbf{x}), \boldsymbol{\sigma}_z(\mathbf{x})) = \text{EncoderNeuralNet}_\phi(\mathbf{x}), \quad (7)$$

$$q_\phi(\mathbf{z} | \mathbf{x}) = \mathcal{N}(\mathbf{z} | \boldsymbol{\mu}_z(\mathbf{x}), \text{diag}(\boldsymbol{\sigma}_z^2(\mathbf{x}))). \quad (8)$$

Here,  $(\boldsymbol{\mu}_z(\mathbf{x}), \boldsymbol{\sigma}_z(\mathbf{x}))$  are the *instance-dependent latent parameters* for the latent code  $\mathbf{z}$ . This inference occurs for every sample  $\mathbf{x}$  and is the key property we aim to exploit.

The decoder is also a Gaussian distribution parameterized by a decoder neural network with parameters  $\theta$ :

$$(\boldsymbol{\mu}_x(\mathbf{z}), \boldsymbol{\sigma}_x(\mathbf{z})) = \text{DecoderNeuralNet}_\theta(\mathbf{z}), \quad (9)$$

$$p_\theta(\mathbf{x} | \mathbf{z}) = \mathcal{N}(\mathbf{x} | \boldsymbol{\mu}_x(\mathbf{z}), \text{diag}(\boldsymbol{\sigma}_x^2(\mathbf{z}))). \quad (10)$$

Here,  $\mathbf{z}$  is sampled from the encoder distribution  $q_\phi(\mathbf{z} | \mathbf{x})$ . The pair  $(\boldsymbol{\mu}_x(\mathbf{z}), \boldsymbol{\sigma}_x(\mathbf{z}))$  represents the *instance-dependent observable parameters* for reconstructing the observation  $\mathbf{x}$ . The reconstruction error is given by  $\|\mathbf{x} - \boldsymbol{\mu}_x(\mathbf{z})\|$ , measuring the difference between the original input and its reconstruction.

## 2.2 VAE REINTERPRETED: THE FAST AND SLOW WEIGHTS PERSPECTIVE

Consider Gaussian VAE learning. Given training data  $\mathbf{X}_{\text{Train}} = \{\mathbf{x}_i\}_{i=1}^N$ , we train an encoder  $q_\phi(\mathbf{z} | \mathbf{x})$  and a decoder  $p_\theta(\mathbf{x} | \mathbf{z})$ :

$$q_\phi(\mathbf{z} | \mathbf{x}) = \mathcal{N}(\mathbf{z} | \boldsymbol{\mu}_z(\mathbf{x}; \phi), \text{diag}(\boldsymbol{\sigma}_z^2(\mathbf{x}; \phi))), \quad (11)$$

$$p_\theta(\mathbf{x} | \mathbf{z}) = \mathcal{N}(\mathbf{x} | \boldsymbol{\mu}_x(\mathbf{z}; \theta), \text{diag}(\boldsymbol{\sigma}_x^2(\mathbf{z}; \theta))). \quad (12)$$

After training, the knowledge in  $\mathbf{X}_{\text{Train}}$  is transferred to  $\phi_{\text{trained}} = \phi(\mathbf{X}_{\text{Train}})$  and  $\theta_{\text{trained}} = \theta(\mathbf{X}_{\text{Train}})$ . This is the first inferential procedure:

$$(\mathbf{X}_{\text{Train}}, q_\phi, p_\theta) \longrightarrow (\phi_{\text{trained}}, \theta_{\text{trained}}) \in (\Phi, \Theta). \quad (13)$$

At test time, when a new observation  $\mathbf{x}_{\text{Test}}$  is given, the encoder and decoder Gaussian parameters are inferred depending on  $\mathbf{x}_{\text{Test}}$ . This is the second inferential procedure:

$$(\mathbf{x}_{\text{Test}}, \phi_{\text{trained}}, \theta_{\text{trained}}) \longrightarrow (\boldsymbol{\mu}_z(\mathbf{x}_{\text{Test}}; \phi_{\text{trained}}), \boldsymbol{\sigma}_z(\mathbf{x}_{\text{Test}}; \phi_{\text{trained}}), \boldsymbol{\mu}_x(\mathbf{z}_{\text{Test}}; \theta_{\text{trained}}), \boldsymbol{\sigma}_x(\mathbf{z}_{\text{Test}}; \theta_{\text{trained}})). \quad (14)$$

There are two kinds of parameters involved. The parameters  $\phi_{\text{trained}}$  and  $\theta_{\text{trained}}$  do not change after training—they are the *slow weights*. The quantities  $\boldsymbol{\mu}_z(\mathbf{x}_{\text{Test}}; \phi_{\text{trained}})$ ,  $\boldsymbol{\sigma}_z(\mathbf{x}_{\text{Test}}; \phi_{\text{trained}})$ ,  $\boldsymbol{\mu}_x(\mathbf{z}_{\text{Test}}; \theta_{\text{trained}})$ ,  $\boldsymbol{\sigma}_x(\mathbf{z}_{\text{Test}}; \theta_{\text{trained}})$  are instance-dependent and are considered the *fast weights* (Hinton & Plaut, 1987; Schmidhuber, 1992; Ba et al., 2016) in our work. From this perspective, the second inferential procedure uses knowledge both from  $\mathbf{X}_{\text{Train}}$  (slow weights) and the test-time instance  $\mathbf{x}_{\text{Test}}$  (fast weights).

Our view is inspired by the connection between multi-head attention in transformers (Schlag et al., 2021) and hypernetworks (Ha et al., 2022), where the instance dependent attention weighting is considered as fast weights parameterizing a (hyper) value network (Schug et al., 2024). In our case, for example, the decoder parameters,  $\boldsymbol{\mu}_x(\mathbf{z}_{\text{Test}}; \theta_{\text{trained}})$ ,  $\boldsymbol{\sigma}_x(\mathbf{z}_{\text{Test}}; \theta_{\text{trained}})$  are fast weights parameterizing a Gaussian distribution which is responsible for evaluating the likelihood of the input  $\mathbf{x}_{\text{Test}}$ .

In the next section, we detail how to use these fast weights  $T(\mathbf{x}, \mathbf{z}) = (\boldsymbol{\mu}_x(\mathbf{z}), \boldsymbol{\sigma}_x(\mathbf{z}), \boldsymbol{\mu}_z(\mathbf{x}), \boldsymbol{\sigma}_z(\mathbf{x}))$  for OOD detection.

## 3 OOD DETECTION WITH FAST AND SLOW WEIGHTS

In this section, we reinterpret a classical prior OOD detection method from the slow weight perspective and introduce our method from the fast weight perspective. We then detail our algorithm. In the next section, we provide a thorough analysis of our method’s statistical and combinatorial foundations.

### 3.1 OOD DETECTION WITH VAE SLOW WEIGHTS

**Reinterpreting the Likelihood Regret Method** The likelihood regret method for OOD detection (Xiao et al., 2020) can be reinterpreted as detecting OOD samples using the information update in slow weights. At a high level, after obtaining  $\theta_{\text{trained}}$  from training, they fine-tune VAEs by maximizing likelihood on a test sample  $\mathbf{x}_{\text{Test}}$  to get  $\theta_{\text{online}}$ , and track the following likelihood regret:

$$\log p(\theta_{\text{online}} | \mathbf{x}_{\text{Test}}) - \log p(\theta_{\text{trained}} | \mathbf{x}_{\text{Test}}). \quad (15)$$

In other words, their work involves two inferential procedures. First,  $(\mathbf{X}_{\text{Train}}, p_\theta) \longrightarrow \theta_{\text{trained}}$ ; second,  $(\mathbf{X}_{\text{Train}}, \mathbf{x}_{\text{Test}}, p_\theta) \longrightarrow \theta_{\text{online}}$ , where they do not maximize  $p_\theta$  jointly on  $(\mathbf{X}_{\text{Train}}, \mathbf{x}_{\text{Test}})$ , but sequentially on  $\mathbf{X}_{\text{Train}}$  first and  $\mathbf{x}_{\text{Test}}$  next. However, likelihood regret is empirically outperformed by alternative approaches (Morningstar et al., 2021) which did not involve any fine-tuning. This is probably because training neural networks on one sample is challenging. Optimizing for a few iterations changes  $\theta_{\text{trained}}$  very little, while training for many iterations results in overfitting quickly. Furthermore, in streaming OOD detection, such computational overhead is formidable.

### 3.2 OOD DETECTION WITH VAE FAST WEIGHTS

Given that OOD detection with slow weights induces formidable computational overhead during test time and poses optimization challenges, we propose to perform OOD detection with fast weights.

In Section 2, we reinterpreted the encoder and decoder means and variances as the fast weights of the VAE:  $T(\mathbf{x}, \mathbf{z}) = (\boldsymbol{\mu}_x(\mathbf{z}), \boldsymbol{\sigma}_x(\mathbf{z}), \boldsymbol{\mu}_z(\mathbf{x}), \boldsymbol{\sigma}_z(\mathbf{x}))$ . However, these remain high-dimensional. This not only increases computational time but can also cause issues for the second-stage statistical algorithm (Maciejewski et al., 2022). We address this problem by taking the L2 norm of  $T(\mathbf{x}, \mathbf{z})$ :

$$u(\mathbf{x}) = \|\mathbf{x} - \hat{\mathbf{x}}\|_2 = \|\mathbf{x} - \boldsymbol{\mu}_x(\boldsymbol{\mu}_z(\mathbf{x}))\|_2, \quad (16)$$

$$v(\mathbf{x}) = \|\boldsymbol{\mu}_z(\mathbf{x})\|_2, \quad (17)$$

$$w(\mathbf{x}) = \|\boldsymbol{\sigma}_z(\mathbf{x})\|_2, \quad (18)$$

$$s(\mathbf{x}) = \|\boldsymbol{\sigma}_x(\boldsymbol{\mu}_z(\mathbf{x}))\|_2. \quad (19)$$

Note that in Eq. 16, instead of taking  $\|\boldsymbol{\mu}_x(\boldsymbol{\mu}_z(\mathbf{x}))\|_2$ , we compute  $\|\mathbf{x} - \boldsymbol{\mu}_x(\boldsymbol{\mu}_z(\mathbf{x}))\|_2$ . This is because  $\|\boldsymbol{\mu}_x(\boldsymbol{\mu}_z(\mathbf{x}))\|_2$  could be unnormalized in magnitude compared to other statistics, causing problems in the second-stage classical density estimation algorithm. Thus, we normalize it by taking the reconstruction error, which should be close to zero due to the VAE optimization objective. While VAE optimization should already be driving Eqs. 17–19 to a small value. Eq. 17 is small, because the KL objective encourages the encoder to be close to prior. Eq. 18 should be close to 1, also due to the KL regularization. Eq. 19 should be small, as model distribution converges weakly to data distribution (Theorem 4 and 5 of Dai & Wipf (2019)).

### 3.3 THE LPATH ALGORITHM FOR FAST WEIGHTS OOD DETECTION

We use Eqs. 16–19 as the scoring metrics for our OOD detection algorithm. We call it the Likelihood Path (LPath) algorithm because it is based on minimal sufficient statistics of the individual components of the factorization of the likelihood function; we provide a detailed description and analysis in Section 4.3.

Our algorithm is detailed in Algorithm 1. It first trains a VAE and extracts statistics in Eqs. 16–19 in the first stage (**neural feature extraction**). Then it fits a classical statistical density estimation algorithm (COPOD (Li et al., 2020) or MD (Lee et al., 2018; Maciejewski et al., 2022)) in the second stage (**classical density estimation**).

Our algorithm can be used with a single VAE model (LPath-1M) or a pair of two models (LPath-2M). For LPath-1M, we use the same VAE to extract all of  $u(\mathbf{x}), v(\mathbf{x}), w(\mathbf{x}), s(\mathbf{x})$ . When used with a pair of two models (LPath-2M), we train two VAEs: one with a very high latent dimension (e.g., 1000) and another with a very low dimension (e.g., 1 or 2). In the second stage, we extract the following statistics:  $(u(\mathbf{x})_{\text{lowD}}, v(\mathbf{x})_{\text{highD}}, w(\mathbf{x})_{\text{highD}}, s(\mathbf{x})_{\text{lowD}})$ , where  $u(\mathbf{x})_{\text{lowD}}, s(\mathbf{x})_{\text{lowD}}$  are taken from the low-dimensional VAE and  $v(\mathbf{x})_{\text{highD}}, w(\mathbf{x})_{\text{highD}}$  from the high-dimensional VAE. Appendix D.1.2 explains the reasoning behind this combination.

## 4 THE LIKELIHOOD PATH PRINCIPLE

In this section, we provide an in-depth analysis of how we arrived at our selected  $T(\mathbf{x}, \mathbf{z}) = (\boldsymbol{\mu}_x(\mathbf{z}), \boldsymbol{\sigma}_x(\mathbf{z}), \boldsymbol{\mu}_z(\mathbf{x}), \boldsymbol{\sigma}_z(\mathbf{x}))$ , the fundamental challenge for this problem, and how to have a general principle to select such statistics not just for VAEs but for other DGMs.

Recall RQ2:

RQ 2: How do we select key statistics for the classical density estimation algorithm?

The goal is to overcome the challenge of dimensionality: If the dimensionality is too high, we might suffer from the curse of dimensionality, but if the dimensionality is too low, we might capture insufficient information to make effective inference. How do we find the sweet spot?

The key idea is our proposed Likelihood Path (LPath) Principle:

Under imperfect likelihood estimation, there is more information in the computational path leading to the marginal likelihood function  $p_\theta(\mathbf{x})$  relative to  $p_\theta(\mathbf{x})$  alone. Information can be optimally extracted by the *minimal sufficient statistics* of the individual components of the factorization of the likelihood function.

**Algorithm 1** Training and Inference: From high-dimensional data to OOD scoring

---

```

1: Input:  $D_{\text{Train, ID}} \sim P_{\text{ID}}$  of size  $n_{\text{train}} \times n_{\text{channels}}$ ,  $D_{\text{Test}} \sim P_{\text{ID}} \cup P_{\text{OOD}}$ 
2: Stage 1 Training: From high-dim dataset to low-dim minimal sufficient statistics
3: Train VAE on  $D_{\text{Train, ID}}$  ▷ Normal training using SGD/Adam
4: for  $\mathbf{x} \in D_{\text{Train, ID}}$  do
5:   Compute and record  $T(\mathbf{x}) = (u(\mathbf{x}), v(\mathbf{x}), w(\mathbf{x}), s(\mathbf{x}))$  ▷ As in Eqs. 16–18
6: end for
7: Create new dataset  $D_{\text{Train, ID, T}}$  of size  $n_{\text{train}} \times 4$  consisting of the minimal sufficient statistics  $T(\mathbf{x})$ 
   for Stage 2 Training
8: Stage 2 Training: From low-dim minimal sufficient statistics to OOD scoring
9: Select classical OOD scoring algorithm  $\mathcal{A}_{\text{Classical}}$  (e.g., COPOD (Li et al., 2020) or MD (Lee
   et al., 2018))
10: Train  $\mathcal{A}_{\text{Classical}}$  on  $D_{\text{Train, ID, T}}$  to get  $\mathcal{A}_{\text{Classical, Trained}}$  ▷ Classical OOD training
11: Inference Stage: OOD Scoring
12: for  $\mathbf{x}_{\text{Test}} \in D_{\text{Test}}$  do
13:   Compute  $T(\mathbf{x}_{\text{Test}}) = (u(\mathbf{x}_{\text{Test}}), v(\mathbf{x}_{\text{Test}}), w(\mathbf{x}_{\text{Test}}), s(\mathbf{x}_{\text{Test}}))$  from trained VAE
14:   Compute OOD score  $S(\mathbf{x}_{\text{Test}}) = \mathcal{A}_{\text{Classical, Trained}}(T(\mathbf{x}_{\text{Test}}))$ 
15: end for
16: Output:  $S(\mathbf{x}_{\text{Test}})$ , an OOD score for each  $\mathbf{x}_{\text{Test}}$ 

```

---

The LPath Principle is a general-purpose principle to select such statistics, and our analysis could also be used to select such statistics for other DGMs; we leave that for future work.

We will start by reviewing the Likelihood Principle and Sufficiency Principle that form the statistical foundation of our proposed LPath Principle.

#### 4.1 THE LIKELIHOOD PRINCIPLE

The maximum likelihood estimation (MLE) approach to unsupervised learning focuses on finding parameters  $\psi$  to maximize the likelihood  $\ell(\psi | \mathbf{x}) := p(\mathbf{x} | \psi)$  given training data  $\mathbf{x}$ , so that we transfer information from  $\mathbf{x}$  to  $\psi$ . MLE is a special case of the *likelihood principle* (Berger & Wolpert, 1988):

The *likelihood principle* states that all the evidence in an observed sample  $\mathbf{x}$  relevant to model parameters is contained in the likelihood function  $\ell(\psi | \mathbf{x})$ .

MLE satisfies the likelihood principle because inferring the most likely parameter depends only on  $\ell(\psi | \mathbf{x})$ . Many OOD detection works (Nalisnick et al., 2019; Xiao et al., 2020) satisfy this principle as well.

*In summary, the likelihood principle postulates that  $\ell(\psi | \mathbf{x})$  (as a function of  $\psi$ ) tells us everything about  $\mathbf{x}$ . If we make our decisions (e.g., OOD detection) based only on the likelihood function, our decision satisfies the likelihood principle.*

#### 4.2 THE SUFFICIENCY PRINCIPLE

While the likelihood principle suggests that all information is contained in  $\ell(\psi | \mathbf{x})$ , it is a complex function and does not directly tell us what statistics to include for RQ2. To better process such overwhelming information, we seek to reduce our selection to the simplest set that still contains sufficient information about  $\ell(\psi | \mathbf{x})$ . How do we formalize such information trimming in the context of unsupervised learning?

- The information reduction procedure  $T$  should be a function of  $\mathbf{x}$ , a *statistic*.
- $T$  should be *sufficient* for describing  $p(\mathbf{x} | \psi)$  or  $\psi$ :  $p(\mathbf{x} | T(\mathbf{x}), \psi) = p(\mathbf{x} | T(\mathbf{x}))$ .
- $T$  should be *minimal*:  $F(T)$  is no longer sufficient for  $\psi$ , for any non-invertible function  $F$ .

In summary, a minimal sufficient statistic  $T$  tells us everything about  $\psi$  that we can possibly learn from observing  $\mathbf{x}$ , and if we attempt to trim  $T$  further by any irreversible process, we would lose some information for inferring  $\ell(\psi | \mathbf{x})^2$ .

Alternatively, we can view sufficient statistics from an information-theoretic perspective. Let  $I$  denote the mutual information.  $T(\mathbf{x})$  is sufficient for  $\psi$  if:

$$I(\psi; T(\mathbf{x})) = I(\psi; \mathbf{x}). \quad (20)$$

In other words, the data processing inequality  $I(\psi; T(\mathbf{x})) \leq I(\psi; \mathbf{x})$  becomes an equality if  $T$  is sufficient. This is useful for answering RQ2. Given a new sample  $\mathbf{x}$ , the encoder and decoder neural nets would produce millions of activations, all of which could be useful for OOD detection. However, this is clearly overwhelming. The minimal sufficient statistic  $T(\mathbf{x})$  gives us the set of statistics that cannot be reduced further without losing some information.

The sample mean vectors and sample covariance matrices (Eqs. 7 and 9) parameterizing the standard Gaussian VAE’s encoder and decoder are *minimal sufficient statistics* (Wasserman, 2006).

### 4.3 LIKELIHOOD PATH PRINCIPLE

Our proposed LPath principle states that:

Under imperfect likelihood estimation, there is more information in the computational path leading to the marginal likelihood function  $p_\theta(\mathbf{x})$  relative to  $p_\theta(\mathbf{x})$  alone. Information can be optimally extracted by the *minimal sufficient statistics* of the individual components of the factorization of the likelihood function.

For VAEs, this entails applying the *likelihood principle* twice in the VAE’s encoder and decoder conditional distributions and tracking their *minimal sufficient statistics*:  $T(\mathbf{x}, \mathbf{z})$ . Here, minimal sufficient statistics represent two **optimal** conditions for inference: They are *sufficient* because once  $(\mu_{\mathbf{z}}(\mathbf{x}), \sigma_{\mathbf{z}}(\mathbf{x}))$  and  $(\mu_{\mathbf{x}}(\mathbf{z}), \sigma_{\mathbf{x}}(\mathbf{z}))$  are known, the conditional likelihood functions can be defined. They are *minimal* because any other parameterization of a Gaussian will involve no fewer parameters.

Recall the VAE formulation:

$$\boxed{\text{LHS has no closed form likelihood nor sufficient statistics.}} \log p_\theta(\mathbf{x}) \approx \log \left[ \frac{p_\theta(\mathbf{x} | \mathbf{z}) p(\mathbf{z})}{q_\phi(\mathbf{z} | \mathbf{x})} \right] \boxed{\text{RHS contains more information given by their minimal sufficient statistics.}} \quad (21)$$

While it is not obvious how to apply likelihood and sufficiency principles to the VAE’s marginal likelihood  $p_\theta(\mathbf{x})$ , we can apply them to the Gaussian VAE’s encoder  $q_\phi(\mathbf{z} | \mathbf{x})$ , prior  $p(\mathbf{z})$ , and decoder  $p_\theta(\mathbf{x} | \mathbf{z})$ , which completely characterize  $p_\theta(\mathbf{x})$ .

Let us make the above precise in our VAE’s LPath. Consider the following Markov chain when we estimate the marginal likelihood of a sample  $\mathbf{x}$ :

$$\mathbf{x} \longrightarrow q_\phi(\mathbf{z} | \mathbf{x}), p(\mathbf{z}), p_\theta(\mathbf{x} | \mathbf{z}) \longrightarrow p_\theta(\mathbf{x}). \quad (22)$$

The data processing inequality from information theory says:

$$I(\mathbf{x}; (q_\phi(\mathbf{z} | \mathbf{x}), p(\mathbf{z}), p_\theta(\mathbf{x} | \mathbf{z}))) \geq I(\mathbf{x}; p_\theta(\mathbf{x})). \quad (23)$$

When density estimation is perfect, the above inequality becomes an equality. In practical cases, perfect learning never happens. Mathematically, our LPath principle thus states:

$$I(\mathbf{x}; (q_\phi(\mathbf{z} | \mathbf{x}), p(\mathbf{z}), p_\theta(\mathbf{x} | \mathbf{z}))) > I(\mathbf{x}; p_\theta(\mathbf{x})). \quad (24)$$

In a nutshell, ***the central theme in our work is to exploit the gap in Inequality 24.***

The chain of information reduction for OOD inference and detection is summarized by Figure 1:

In the first column of Figure 1, it is hard to define a metric in the visible space to distinguish  $\mathbf{x}_{\text{ID}}$  and  $\mathbf{x}_{\text{OOD}}$ , even though they contain the most evidence. In the second column, we compare them by comparing their corresponding likelihood functions, suggested by the likelihood principle. The third column compares their maximum likelihood inferences. The last column suggests that it suffices to know the sufficient statistics  $T$  to obtain  $\theta_{\text{MLE}}$ , which completes the information reduction chain.

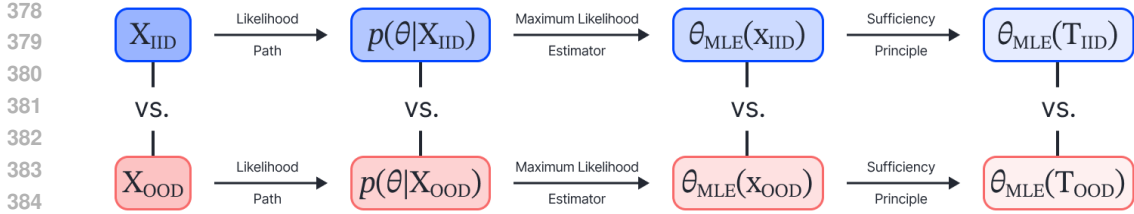


Figure 1: Left to right shows the information reduction via the likelihood principle (LP), maximum likelihood estimation (MLE), and sufficiency principle (SP).  $T$  denotes sufficient statistics. The top and bottom rows contrast inferences between  $x_{ID}$  and  $x_{OOD}$ .

ID OOD	CIFAR10				SVHN			FMNIST			MNIST		
	SVHN	CIFAR100	Hflip	Vflip	CIAFR10	Hflip	Vflip	MNIST	Hflip	Vflip	FMNIST	Hflip	Vflip
ELBO	0.08	0.54	0.5	0.56	<b>0.99</b>	0.5	0.5	0.87	0.63	0.83	<b>1.00</b>	0.59	0.6
LR (Xiao et al., 2020)	0.88	N/A	N/A	N/A	0.92	N/A	N/A	0.99	N/A	N/A	N/A	N/A	N/A
BIVA (Havtorn et al., 2021)	0.89	N/A	N/A	N/A	<b>0.99</b>	N/A	N/A	0.98	N/A	N/A	<b>1.00</b>	N/A	N/A
DoSE (Morningstar et al., 2021)	0.97	0.57	0.51	0.53	<b>0.99</b>	0.52	0.51	<b>1.00</b>	0.66	0.75	<b>1.00</b>	<b>0.81</b>	0.83
Fisher (Bergamin et al., 2022)	0.87	0.59	N/A	N/A	N/A	N/A	N/A	0.96	N/A	N/A	N/A	N/A	N/A
DDPM (Liu et al., 2023)	0.98	N/A	0.51	0.63	<b>0.99</b>	<b>0.62</b>	<b>0.58</b>	0.97	0.65	<b>0.89</b>	N/A	N/A	N/A
LMD (Graham et al., 2023)	<b>0.99</b>	0.61	N/A	N/A	0.91	N/A	N/A	0.99	N/A	N/A	<b>1.00</b>	N/A	N/A
LPath-1M-COPOD (Ours)	<b>0.99</b>	<b>0.62</b>	<b>0.53</b>	0.61	<b>0.99</b>	0.55	0.56	<b>1.00</b>	0.65	0.81	<b>1.00</b>	0.65	<b>0.87</b>
LPath-2M-COPOD (Ours)	0.98	<b>0.62</b>	<b>0.53</b>	<b>0.65</b>	0.96	0.56	0.55	0.95	<b>0.67</b>	0.87	<b>1.00</b>	0.77	0.78
LPath-1M-MD (Ours)	<b>0.99</b>	0.58	0.52	0.60	0.95	0.52	0.52	0.97	0.63	0.82	<b>1.00</b>	0.75	0.76

Table 1: AUROC of OOD Detection with different ID and OOD datasets. LPath-1M is LPath with one model, LPath-2M is LPath with two models.

#### 4.4 COMBINATORIAL CANCELLATION

We analyzed the LPath Principle for OOD detection from the statistical perspective. We can gain more concrete insights on why the LPath Principle works if we take a combinatorial perspective, which can act as an empirical method to select statistics, answering RQ2. The key insight is that factors in the likelihood function risk **getting canceled** in the likelihood itself, and the signals they contain for OOD detection will be drowned out. This is how information is lost in Eq. 24. To address this, we could separate each factor out and capture the signal they contain with their sufficient statistics, arriving at our LPath Principle.

In the case of VAEs, the encoder and decoder contain complementary information for OOD detection, but they could be canceled out in  $\log p_\theta(\mathbf{x})$ . Recall the VAE’s likelihood estimation:  $\log p_\theta(\mathbf{x}) \approx \log \left[ \frac{p_\theta(\mathbf{x}|\mathbf{z})p(\mathbf{z})}{q_\phi(\mathbf{z}|\mathbf{x})} \right]$ . The decoder’s conditional likelihood  $p_\theta(\mathbf{x}|\mathbf{z})$  being too large and prior  $p(\mathbf{z})$  (evaluated at samples from the encoder  $q_\phi(\mathbf{z}|\mathbf{x})$ ) being too small both suggest  $\mathbf{x}$  could be an anomaly, but their scalar product can be well-ranged, which drowns out the signal for OOD discovery. A more concrete interpretation of this cancellation phenomenon from the pixel texture vs. semantics perspective can be found in Appendix B.

For  $x_{ID}$  and  $x_{OOD}$ , we would anticipate different likelihood paths. This difference can be detected by their corresponding sufficient statistics:  $T(x_{ID}, z_{ID}) = (\mu_x(z_{ID}), \sigma_x(z_{ID}), \mu_z(x_{ID}), \sigma_z(x_{ID}))$  and  $T(x_{OOD}, z_{OOD}) = (\mu_x(z_{OOD}), \sigma_x(z_{OOD}), \mu_z(x_{OOD}), \sigma_z(x_{OOD}))$ . In other words, a new sample may be considered as ID if its sufficient statistics are similar to  $T(x_{ID}, z_{ID})$  for some  $x_{ID} \in P_{ID}$  (because the encoder and decoder distributions are completely characterized by  $T$ ).

## 5 EXPERIMENTS

We compare our methods with state-of-the-art OOD detection methods (Kirichenko et al., 2020; Xiao et al., 2020; Havtorn et al., 2021; Morningstar et al., 2021; Bergamin et al., 2022; Liu et al., 2023; Graham et al., 2023), under the unsupervised, single batch, no data inductive bias assumption setting.



432 Following the convention in those methods, we have conducted experiments with a number of  
 433 common benchmarks, including CIFAR10 (Krizhevsky & Hinton, 2009), SVHN (Netzer et al.,  
 434 2011), CIFAR100 (Krizhevsky & Hinton, 2009), MNIST (LeCun et al., 1998), FashionMNIST  
 435 (FMNIST) (Xiao et al., 2017), and their horizontally flipped and vertically flipped variants.  
 436

437 **Experimental Results.** Table 1 show that our methods surpass or are on par with the state-of-the-art  
 438 (SOTA). Because our setting assumes no access to labels, batches of test data, or any inductive bias  
 439 on the dataset, OOD datasets like Hflip and Vflip become very challenging. Most prior methods  
 440 achieved only near-chance AUROC on Vflip and Hflip for CIFAR10 and SVHN as ID data. This is  
 441 expected because horizontally flipped CIFAR10 or SVHN differs from the in-distribution only by one  
 442 latent dimension. Even so, our methods still managed to surpass prior SOTA in some cases, though  
 443 only marginally. More experimental details, including various ablation studies, are in Appendix D, E.

444 **Achieving More with Less.** This improvement is more significant given that we only used a  
 445 very small VAE architecture. Compared to other SOTA methods, we used a much smaller model  
 446 (DC-VAEs from (Xiao et al., 2020)’s architecture) with a parameter count of **3M**, compared to **44M**  
 447 for Glow (Kingma & Dhariwal, 2018) in DoSE (Morningstar et al., 2021) and **46M** for the diffusion  
 448 model (Rombach et al., 2022; Liu et al., 2023). Specifically, our method clearly exceeds other  
 449 VAE-based methods (Xiao et al., 2020; Havtorn et al., 2021), and is the only VAE-based method  
 450 that is competitive against bigger models. DoSE (Morningstar et al., 2021) conducted experiments  
 451 on VAEs with five carefully chosen statistics. They reported their MNIST/FMNIST results on their  
 452 VAEs and used Glow on more difficult datasets like CIFAR/SVHN. We assume the reason is that  
 453 Glow performed better on more complex datasets. Our methods surpass their Glow-based results,  
 454 which should, in turn, be better than their method applied to VAEs. On one hand, Glow’s likelihood  
 455 is arguably much better estimated than our small DC-VAE model. On the other hand, their statistics  
 456 appear to be more sophisticated. However, our simple method manages to surpass their scores. This  
 457 showcases the efficiency and effectiveness of our method.  
 458

## 459 6 RELATED WORK

460  
 461 In this section, we discuss related OOD detection methods that are under the same settings with ours.  
 462 For more related works on other OOD detection settings, see Appendix A.

463 As mentioned in Section 1, our method is among the most general and difficult settings where we  
 464 assume no access to labels, batches of test data, or any inductive bias of the dataset (Xiao et al., 2020;  
 465 Kirichenko et al., 2020; Havtorn et al., 2021; Ahmadian & Lindsten, 2021; Morningstar et al., 2021;  
 466 Bergamin et al., 2022; Liu et al., 2023; Graham et al., 2023). Xiao et al. (2020) fine-tune the VAE  
 467 encoders on the test data and take the likelihood ratio as the OOD score. Kirichenko et al. (2020)  
 468 trained RealNVP on EfficientNet (Tan & Le, 2020) embeddings and use log-likelihood directly as  
 469 the OOD score. Havtorn et al. (2021) trained hierarchical VAEs such as HVAE and BIVA and used  
 470 the log-likelihood directly as the OOD score. We compare our method with the above methods in  
 471 Table 1.

472 Some recent works on OOD detection (Ahmadian & Lindsten, 2021; Bergamin et al., 2022; Morn-  
 473 ingstar et al., 2021; Graham et al., 2023; Liu et al., 2023; Osada et al., 2023) indeed start to consider  
 474 other information contained in the entire neural activation path leading to the likelihood. Examples  
 475 include entropy, KL divergence, and Jacobian in the likelihood (Morningstar et al., 2021). However,  
 476 they do not address RQ2 and provide a principled method to select such statistics.  
 477

## 478 7 CONCLUSION

479  
 480 We presented the Likelihood Path Principle applied to unsupervised, one-sample OOD detection. We  
 481 provided in-depth analyses from the neural (fast-slow weights), statistical (likelihood and sufficiency  
 482 principles), and combinatorial (cancellation effect) perspectives. Our method is principled and  
 483 supported by SOTA results. In future work, we plan to adapt our principles and techniques to more  
 484 powerful DGMs, such as Glow or diffusion models.  
 485

## REFERENCES

- 486  
487  
488 Amirhossein Ahmadian and Fredrik Lindsten. Likelihood-free out-of-distribution detection with  
489 invertible generative models. In Zhi-Hua Zhou (ed.), *Proceedings of the Thirtieth International*  
490 *Joint Conference on Artificial Intelligence, IJCAI-21*, pp. 2119–2125. International Joint Con-  
491 ferences on Artificial Intelligence Organization, 8 2021. doi: 10.24963/ijcai.2021/292. URL  
492 <https://doi.org/10.24963/ijcai.2021/292>. Main Track.
- 493 Jimmy Ba, Geoffrey E Hinton, Volodymyr Mnih, Joel Z Leibo, and Catalin Ionescu. Using fast  
494 weights to attend to the recent past. *Advances in neural information processing systems*, 29, 2016.
- 495  
496 Dara Bahri, Heinrich Jiang, Yi Tay, and Donald Metzler. Label smoothed embedding hypothesis for  
497 out-of-distribution detection, 2021.
- 498 Jens Behrmann, Paul Vicol, Kuan-Chieh Wang, Roger Grosse, and Jörn-Henrik Jacobsen. Understand-  
499 ing and mitigating exploding inverses in invertible neural networks. In *International Conference*  
500 *on Artificial Intelligence and Statistics*, pp. 1792–1800. PMLR, 2021.
- 501  
502 Federico Bergamin, Pierre-Alexandre Mattei, Jakob Drachmann Havtorn, Hugo Senetaire, Hugo  
503 Schmutz, Lars Maaløe, Soren Hauberg, and Jes Frellesen. Model-agnostic out-of-distribution  
504 detection using combined statistical tests. In *International Conference on Artificial Intelligence*  
505 *and Statistics*, pp. 10753–10776. PMLR, 2022.
- 506 James O Berger and Robert L Wolpert. The likelihood principle. IMS, 1988.
- 507  
508 Milan Cvitkovic and Günther Koliander. Minimal achievable sufficient statistic learning. In *Interna-*  
509 *tional Conference on Machine Learning*, pp. 1465–1474. PMLR, 2019.
- 510 Bin Dai and David Wipf. Diagnosing and enhancing vae models. *arXiv preprint arXiv:1903.05789*,  
511 2019.
- 512  
513 Bin Dai, Li Kevin Wenliang, and David Wipf. On the value of infinite gradients in variational  
514 autoencoder models. In *Advances in Neural Information Processing Systems*.
- 515  
516 Carl Doersch. Tutorial on variational autoencoders. *arXiv preprint arXiv:1606.05908*, 2016.
- 517  
518 Nicholas Frosst, Nicolas Papernot, and Geoffrey Hinton. Analyzing and improving representations  
519 with the soft nearest neighbor loss, 2019.
- 520  
521 Mark S Graham, Walter HL Pinaya, Petru-Daniel Tudosiu, Parashkev Nachev, Sebastien Ourselin,  
522 and Jorge Cardoso. Denoising diffusion models for out-of-distribution detection. In *Proceedings*  
523 *of the IEEE/CVF Conference on Computer Vision and Pattern Recognition*, pp. 2947–2956, 2023.
- 524  
525 Arthur Gretton, Karsten M Borgwardt, Malte J Rasch, Bernhard Schölkopf, and Alexander Smola. A  
526 kernel two-sample test. *The Journal of Machine Learning Research*, 13(1):723–773, 2012.
- 527  
528 Théo Guénais, Dimitris Vamvourellis, Yaniv Yacoby, Finale Doshi-Velez, and Weiwei Pan. Bacoun:  
529 Bayesian classifiers with out-of-distribution uncertainty. *arXiv preprint arXiv:2007.06096*, 2020.
- 530  
531 David Ha, Andrew M Dai, and Quoc V Le. Hypernetworks. In *International Conference on Learning*  
532 *Representations*, 2022.
- 533  
534 Jakob D Drachmann Havtorn, Jes Frellesen, Soren Hauberg, and Lars Maaløe. Hierarchical vases know  
535 what they don’t know. In *International Conference on Machine Learning*, pp. 4117–4128. PMLR,  
536 2021.
- 537  
538 Dan Hendrycks and Kevin Gimpel. A baseline for detecting misclassified and out-of-distribution  
539 examples in neural networks. *arXiv preprint arXiv:1610.02136*, 2016.
- 536  
537 Geoffrey E Hinton and David C Plaut. Using fast weights to deblur old memories. In *Proceedings of*  
538 *the ninth annual conference of the Cognitive Science Society*, pp. 177–186, 1987.
- 539  
539 Agnan Kessy, Alex Lewin, and Korbinian Strimmer. Optimal whitening and decorrelation. *The*  
*American Statistician*, 72(4):309–314, 2018.

- 540 Diederik P Kingma and Max Welling. Auto-encoding variational bayes. *arXiv preprint*  
541 *arXiv:1312.6114*, 2013.
- 542 Diederik P Kingma, Max Welling, et al. An introduction to variational autoencoders. *Foundations*  
543 *and Trends® in Machine Learning*, 12(4):307–392, 2019.
- 544 Durk P Kingma and Prafulla Dhariwal. Glow: Generative flow with invertible 1x1 convolutions.  
545 *Advances in neural information processing systems*, 31, 2018.
- 546 Polina Kirichenko, Pavel Izmailov, and Andrew G Wilson. Why normalizing flows fail to detect  
547 out-of-distribution data. *Advances in neural information processing systems*, 33:20578–20589,  
548 2020.
- 549 Alex Krizhevsky and Geoffrey Hinton. Learning multiple layers of features from tiny images.  
550 Technical report, Citeseer, 2009.
- 551 Balaji Lakshminarayanan, Alexander Pritzel, and Charles Blundell. Simple and scalable predictive  
552 uncertainty estimation using deep ensembles. *arXiv preprint arXiv:1612.01474*, 2016.
- 553 Charline Le Lan and Laurent Dinh. Perfect density models cannot guarantee anomaly detection.  
554 *Entropy*, 23(12):1690, 2021.
- 555 Yann LeCun, Léon Bottou, Yoshua Bengio, and Patrick Haffner. Gradient-based learning applied to  
556 document recognition. *Proceedings of the IEEE*, 86(11):2278–2324, 1998.
- 557 Kimin Lee, Kibok Lee, Honglak Lee, and Jinwoo Shin. A simple unified framework for detecting  
558 out-of-distribution samples and adversarial attacks. *Advances in neural information processing*  
559 *systems*, 31, 2018.
- 560 Zheng Li, Yue Zhao, Nicola Botta, Cezar Ionescu, and Xiyang Hu. Copod: copula-based outlier  
561 detection. In *2020 IEEE International Conference on Data Mining (ICDM)*, pp. 1118–1123. IEEE,  
562 2020.
- 563 Zhenzhen Liu, Jin Peng Zhou, Yufan Wang, and Kilian Q Weinberger. Unsupervised out-of-  
564 distribution detection with diffusion inpainting. *arXiv preprint arXiv:2302.10326*, 2023.
- 565 Henryk Maciejewski, Tomasz Walkowiak, and Kamil Szyk. Out-of-distribution detection in high-  
566 dimensional data using mahalanobis distance-critical analysis. In *Computational Science–ICCS*  
567 *2022: 22nd International Conference, London, UK, June 21–23, 2022, Proceedings, Part I*, pp.  
568 262–275. Springer, 2022.
- 569 Warren Morningstar, Cusuh Ham, Andrew Gallagher, Balaji Lakshminarayanan, Alex Alemi, and  
570 Joshua Dillon. Density of states estimation for out of distribution detection. In *International*  
571 *Conference on Artificial Intelligence and Statistics*, pp. 3232–3240. PMLR, 2021.
- 572 Tsendsuren Munkhdalai and Adam Trischler. Metalearning with hebbian fast weights. *CoRR*,  
573 abs/1807.05076, 2018. URL <http://arxiv.org/abs/1807.05076>.
- 574 Eric Nalisnick, Akihiro Matsukawa, Yee Whye Teh, Dilan Gorur, and Balaji Lakshminarayanan. Do  
575 deep generative models know what they don’t know? *arXiv preprint arXiv:1810.09136*, 2018.
- 576 Eric Nalisnick, Akihiro Matsukawa, Yee Whye Teh, and Balaji Lakshminarayanan. Detecting out-of-  
577 distribution inputs to deep generative models using typicality. *arXiv preprint arXiv:1906.02994*,  
578 2019.
- 579 Yuval Netzer, Tao Wang, Adam Coates, Alessandro Bissacco, Bo Wu, and Andrew Y Ng. Reading  
580 digits in natural images with unsupervised feature learning. 2011.
- 581 Genki Osada, Tsubasa Takahashi, Budrul Ahsan, and Takashi Nishide. Out-of-distribution detection  
582 with reconstruction error and typicality-based penalty. In *Proceedings of the IEEE/CVF Winter*  
583 *Conference on Applications of Computer Vision*, pp. 5551–5563, 2023.
- 584 Kazuki Osawa, Siddharth Swaroop, Anirudh Jain, Runa Eschenhagen, Richard E Turner, Rio Yokota,  
585 and Mohammad Emtiyaz Khan. Practical deep learning with bayesian principles. *arXiv preprint*  
586 *arXiv:1906.02506*, 2019.

- 594 Nicolas Papernot and Patrick McDaniel. Deep k-nearest neighbors: Towards confident, interpretable  
595 and robust deep learning, 2018.  
596
- 597 Tim Pearce, Felix Leibfried, and Alexandra Brintrup. Uncertainty in neural networks: Approximately  
598 bayesian ensembling. In *International conference on artificial intelligence and statistics*, pp.  
599 234–244. PMLR, 2020.
- 600 Jie Ren, Peter J Liu, Emily Fertig, Jasper Snoek, Ryan Poplin, Mark Depristo, Joshua Dillon, and  
601 Balaji Lakshminarayanan. Likelihood ratios for out-of-distribution detection. In *Advances in  
602 Neural Information Processing Systems*, pp. 14707–14718, 2019.  
603
- 604 Robin Rombach, Andreas Blattmann, Dominik Lorenz, Patrick Esser, and Björn Ommer. High-  
605 resolution image synthesis with latent diffusion models. In *Proceedings of the IEEE/CVF confer-  
606 ence on computer vision and pattern recognition*, pp. 10684–10695, 2022.
- 607 Chandramouli Shama Sastry and Sageev Oore. Detecting out-of-distribution examples with Gram  
608 matrices. In Hal Daumé III and Aarti Singh (eds.), *Proceedings of the 37th International Conference  
609 on Machine Learning*, volume 119 of *Proceedings of Machine Learning Research*, pp. 8491–8501.  
610 PMLR, 13–18 Jul 2020.
- 611 Imanol Schlag, Kazuki Irie, and Jürgen Schmidhuber. Linear transformers are secretly fast weight  
612 programmers. In *International Conference on Machine Learning*, pp. 9355–9366. PMLR, 2021.  
613
- 614 Jürgen Schmidhuber. Learning to control fast-weight memories: An alternative to dynamic recurrent  
615 networks. *Neural Computation*, 4(1):131–139, 1992.
- 616 Simon Schug, Seijin Kobayashi, Yassir Akram, João Sacramento, and Razvan Pascanu. Attention as  
617 a hypernetwork. *arXiv preprint arXiv:2406.05816*, 2024.  
618
- 619 Joan Serrà, David Álvarez, Vicenç Gómez, Olga Slizovskaia, José F Núñez, and Jordi Luque.  
620 Input complexity and out-of-distribution detection with likelihood-based generative models. In  
621 *International Conference on Learning Representations*, 2019.
- 622 Mingxing Tan and Quoc V. Le. Efficientnet: Rethinking model scaling for convolutional neural  
623 networks, 2020.  
624
- 625 Larry Wasserman. *All of nonparametric statistics*. Springer Science & Business Media, 2006.  
626
- 627 Han Xiao, Kashif Rasul, and Roland Vollgraf. Fashion-mnist: a novel image dataset for benchmarking  
628 machine learning algorithms. *arXiv preprint arXiv:1708.07747*, 2017.
- 629 Zhisheng Xiao, Qing Yan, and Yali Amit. Likelihood regret: An out-of-distribution detection score  
630 for variational auto-encoder. *Advances in neural information processing systems*, 33:20685–20696,  
631 2020.
- 632 Lily Zhang, Mark Goldstein, and Rajesh Ranganath. Understanding Failures in Out-of-Distribution  
633 Detection with Deep Generative Models. In *Proceedings of the 38th International Conference on  
634 Machine Learning*, pp. 12427–12436. PMLR, July 2021. URL [https://proceedings.mlr.  
635 press/v139/zhang21g.html](https://proceedings.mlr.press/v139/zhang21g.html). ISSN: 2640-3498.  
636  
637  
638  
639  
640  
641  
642  
643  
644  
645  
646  
647

## A MORE RELATED WORKS

Prior works have approached OOD detection from various perspectives and with different data assumptions, e.g., with or without access to training labels, batches of test data, or single test data points in a streaming fashion, and with or without knowledge and inductive bias of the data. In the following, we give an overview organized by different data assumptions with a focus on where our method fits.

The first assumption is whether the method has access to training labels. There has been extensive work on classifier-based methods that assume access to training labels (Hendrycks & Gimpel, 2016; Frosst et al., 2019; Sastry & Oore, 2020; Bahri et al., 2021; Papernot & McDaniel, 2018; Osawa et al., 2019; Guénais et al., 2020; Lakshminarayanan et al., 2016; Pearce et al., 2020). Within this category, there are different assumptions as well, such as access to a pretrained network or knowledge of OOD test examples. See Table 1 of Sastry & Oore (2020) for a summary of such methods.

When we do not assume access to the training labels, the problem becomes more general and also harder. Under this category, some methods assume access to a batch of test data where either all the data points are OOD or not (Nalisnick et al., 2019). A more general setting does not assume OOD data would come in batches. Under this setup, there are methods that implicitly assume prior knowledge of the data, such as the input complexity method (Serrà et al., 2019), where the use of image compressors implicitly assumes an image-like structure, or the likelihood ratio method (Ren et al., 2019), where a noisy background model is trained with the assumption of a background-object structure.

## B INTERPRETATION OF LIKELIHOOD CANCELLATION

Recall VAEs’ likelihood estimation (parameterized by  $\theta$ ):

$$\log p_{\theta}(\mathbf{x}) \approx \log \left[ \frac{p_{\theta}(\mathbf{x} | \mathbf{z}) p(\mathbf{z})}{q_{\phi}(\mathbf{z} | \mathbf{x})} \right], \quad (25)$$

The decoder  $p_{\theta}(\mathbf{x} | \mathbf{z})$ ’s reconstruction focuses on the pixel textures, while encoder  $q_{\phi}(\mathbf{z} | \mathbf{x})$ ’s samples evaluated at the prior,  $p(\mathbf{z})$ , describe semantics. Consider  $\mathbf{x}_{\text{OOD}}$ , whose lower level features are similar to ID data, but is semantically different. We can imagine  $p_{\theta}(\mathbf{x} | \mathbf{z})$  is large while  $p(\mathbf{z})$  is small. However, (Havtorn et al., 2021) demonstrates  $p_{\theta}(\mathbf{x})$  is dominated by lower level information. Even if  $p(\mathbf{z})$  wants to reveal  $\mathbf{x}_{\text{OOD}}$ ’s OOD nature, we cannot decipher it through  $p_{\theta}(\mathbf{x}_{\text{OOD}})$ . The converse:  $p_{\theta}(\mathbf{x} | \mathbf{z})$  can flag  $\mathbf{x}_{\text{OOD}}$  when the reconstruction error is big. But if  $p(\mathbf{z})$  is unusually high compared to typical  $\mathbf{x}_{\text{ID}}$ ,  $p_{\theta}(\mathbf{x})$  may appear less OOD.

## C SUFFICIENT STATISTICS AND WHERE TO FIND THEM

Though in the case of the Gaussian parameterized VAE decoder and encoder, it is easy to find the corresponding minimal sufficient statistics, the same might not be true for more complicated distributions. Here we briefly overview the Fisher-Neyman factorization perspective on the sufficiency principle which can help find sufficient statistics in more complicated distributions. A sufficiency principle is also characterized by Fisher-Neyman factorization theorem (Wasserman, 2006):  $T(\mathbf{x})$  is a sufficient statistics for  $p(\mathbf{x}|\psi)$  parameterized by  $\psi$  if and only if:

$$\ell(\psi|\mathbf{x}) = p(\mathbf{x}|\psi) = f(\mathbf{x})g_{\psi}(T(\mathbf{x})) \quad (26)$$

i.e. the density  $p(\mathbf{x}|\psi)$  can be factored into a product such that  $f$ , does not depend on  $\psi$  and  $g$  that does depend on  $\psi$  but *who depends on  $\mathbf{x}$  only through  $T(\mathbf{x})$* . For example, if we perform inference by maximum likelihood:

$$\psi_{\text{MLE}} = \arg \max_{\psi} \ell(\psi|\mathbf{x}) = \arg \max_{\psi} f(\mathbf{x})g_{\psi}(T(\mathbf{x})) = \arg \max_{\psi} g_{\psi}(T) \quad (27)$$

$T$  is sufficient for MLE procedure, because  $\psi_{\text{MLE}}$  only requires  $T$ .

The *sufficiency principle* states that, if  $T(\mathbf{x})$  is a sufficient statistic for the likelihood function  $p(\psi|\mathbf{x})$ , then any inference about  $\psi$  should depend on  $T(\mathbf{x})$  only.

## 702 D EXPERIMENTAL DETAILS

### 703 D.1 VAE ARCHITECTURE AND TRAINING

704 For the architecture and the training of our VAEs, we followed Xiao et al. (2020). In addition,  
 705 we have trained VAEs of varying latent dimensions,  $\{1, 2, 5, 10, 100, 1000, 2000, 3096, 5000, 10000\}$ ,  
 706 and instead of training for 200 epochs and taking the resulting model checkpoint, we took  
 707 the checkpoint that had the best validation loss. For LPath-1M, we conducted experiments on VAEs  
 708 with all latent dimensions and for LPath-2M, we paired one high-dimensional VAE from the group  
 709  $\{3096, 5000, 10000\}$  and one low-dimensional VAE from the group  $\{1, 2, 5\}$ .

710 In addition to Gaussian VAEs as mentioned in Section D.1.3, we also empirically experimented with  
 711 a categorical decoder, in the sense the decoder output is between the discrete pixel ranges, as in Xiao  
 712 et al. (2020). Strictly speaking, this no longer satisfies the Gaussian distribution anymore, which  
 713 may in turn violate our sufficient statistics perspective. However, we still experimented with it to  
 714 test whether LPath principles can be interpreted as a heuristic to inspire methods that approximate  
 715 sufficient statistics that can work reasonably well, and we observed that categorical decoders work  
 716 similarly with Gaussian decoders.

#### 717 D.1.1 DIMENSIONALITY TRADE-OFF

718 In this section, we discuss heuristics for training VAEs in the context of OOD detection, focusing on  
 719 the trade-offs involved in selecting the latent dimension.

720 **Balancing the Trade-off in Latent Dimension** A single VAE encounters a trade-off when selecting  
 721 the latent dimension for effective OOD detection:

- 722 • **Higher Latent Dimension Benefits the Encoder:** Increasing the latent dimension enhances  
 723 the encoder’s ability  $q_\phi$  to discriminate between in-distribution (ID) and OOD data. A  
 724 higher-dimensional latent space allows the encoder to map ID and OOD data to more  
 725 distinct regions, reducing overlap and improving separability. This increased capacity  
 726 enables the encoder to capture complex features of the data, improving its discriminative  
 727 power.
- 728 • **Lower Latent Dimension Benefits the Decoder:** Decreasing the latent dimension en-  
 729 hances the decoder’s ability  $p_\theta$  to identify OOD data through reconstruction errors. A  
 730 lower-dimensional latent space constrains the decoder, making it less capable of accurately  
 731 reconstructing OOD data that it hasn’t seen during training. This constraint leads to larger  
 732 reconstruction errors  $u(\mathbf{x}) = \|\mathbf{x} - \hat{\mathbf{x}}\|_2$  for OOD samples, providing a useful signal for  
 733 detection.

734 This trade-off poses a challenge: adjusting the latent dimension to favor one component (encoder or  
 735 decoder) may compromise the performance of the other. Increasing the latent dimension benefits  
 736 the encoder but may reduce the decoder’s effectiveness in generating meaningful reconstruction  
 737 errors. Conversely, decreasing the latent dimension enhances the decoder’s ability to produce larger  
 738 reconstruction errors for OOD data but may impair the encoder’s discriminative capacity.

739 **Implications for VAE Design** When designing a single VAE for OOD detection, it’s essential to  
 740 consider this trade-off:

- 741 • **For the Encoder:** Aim for a higher latent dimension to improve the separation between ID  
 742 and OOD data in the latent space.
- 743 • **For the Decoder:** Consider a lower latent dimension to increase reconstruction errors for  
 744 OOD data, enhancing detection based on reconstruction discrepancies.

745 However, finding an optimal latent dimension that satisfies both requirements within a single VAE  
 746 can be challenging. Adjusting the latent dimension to favor one aspect inherently affects the other,  
 747 leading to suboptimal performance in at least one component.

**Two VAEs Face No Such Trade-off** To overcome this trade-off inherent in a single VAE, we propose using two VAEs with different latent dimensions, as discussed in the next section. By pairing a high-dimensional VAE with a low-dimensional one, we can leverage the strengths of both models without being constrained by the conflicting requirements of a single latent dimension.

#### D.1.2 PAIRING VAES: LEVERAGING DUAL LATENT DIMENSIONS

**Two VAEs Overcome the Trade-off** To resolve the trade-off in latent dimension selection, we propose training two VAEs with different latent dimensions:

1. **High-Dimensional VAE:** This VAE has an overparameterized (large) latent dimension. Its encoder  $q_\phi$  is capable of capturing complex features and provides informative statistics such as  $v(\mathbf{x})$  and  $w(\mathbf{x})$  that help discriminate between ID and OOD data.
2. **Low-Dimensional VAE:** This VAE has an underparameterized (small) latent dimension. Its decoder  $p_\theta$  is constrained, leading to higher reconstruction errors  $u(\mathbf{x})$  for OOD data due to its limited capacity to represent unfamiliar inputs.

By combining the strengths of both VAEs, we can effectively detect OOD data. The high-dimensional VAE’s encoder excels at distinguishing ID from OOD data in the latent space, while the low-dimensional VAE’s decoder amplifies reconstruction errors for OOD samples.

**Implementation Details** In practice, we extract the following statistics:

- **From the High-Dimensional VAE:**

$$v(\mathbf{x}) = \|\boldsymbol{\mu}_z(\mathbf{x})\|_2, \quad (28)$$

$$w(\mathbf{x}) = \|\boldsymbol{\sigma}_z(\mathbf{x})\|_2, \quad (29)$$

where  $\boldsymbol{\mu}_z(\mathbf{x})$  and  $\boldsymbol{\sigma}_z(\mathbf{x})$  are the encoder’s mean and standard deviation in the latent space.

- **From the Low-Dimensional VAE:**

$$u(\mathbf{x}) = \|\mathbf{x} - \hat{\mathbf{x}}\|_2, \quad (30)$$

$$s(\mathbf{x}) = \|\boldsymbol{\sigma}_x(\boldsymbol{\mu}_z(\mathbf{x}))\|_2, \quad (31)$$

where  $\hat{\mathbf{x}}$  is the reconstructed input, and  $\boldsymbol{\sigma}_x(\boldsymbol{\mu}_z(\mathbf{x}))$  is the decoder’s standard deviation.

By integrating these statistics, we create a comprehensive feature set for OOD detection that leverages both the encoder’s discriminative ability and the decoder’s reconstruction error signal.

**Empirical Results** This approach has led to improvements in challenging OOD detection scenarios. For instance, when training on CIFAR-10 as the in-distribution dataset and using CIFAR-100, vertically flipped (VFlip), and horizontally flipped (HFlip) images as OOD datasets, our method achieved state-of-the-art results.

Remarkably, this was accomplished even though both VAEs, when considered individually, might have limitations:

- The **Overparameterized VAE** (high latent dimension) may overfit the training data, potentially reducing its generalization to unseen data.
- The **Underparameterized VAE** (low latent dimension) may struggle to reconstruct even some ID data accurately due to its limited capacity.

However, by combining their complementary strengths, we surpassed the performance of larger model architectures specifically designed for image data (see Table 1).

Pairing two VAEs with different latent dimensions allows us to capitalize on the advantages of both high and low-dimensional latent spaces without being constrained by the trade-offs inherent in a single model. This strategy provides a practical and effective solution for improving OOD detection performance, demonstrating that sometimes “it takes two to transcend.”

### 810 D.1.3 CONSTANT DECODER COVARIANCE

811  
812 In typical VAE learning, the decoder’s variance is fixed Dai et al., so it cannot be used as an inferential  
813 parameter. We initially treated the decoder as an isotropic Gaussian with a learnable scalar covariance  
814 matrix  $\sigma_{\mathbf{x}}(\mathbf{z})^2 I$ , where  $I$  is the identity matrix and  $\sigma_{\mathbf{x}}(\mathbf{z})^2$  is a learnable scalar. We later observed  
815 that the scalar  $\sigma_{\mathbf{x}}(\mathbf{z})$  always converge to a small value and remains fixed for any ID or OOD data.  
816 And given that in typical VAE learning, the decoder’s variance is fixed Dai et al.. We decided to use a  
817 fixed scalar as well and exclude this term from our algorithm.

818 This reduces the minimal sufficient statistics for encoder and decoder pair:

$$819 (\mu_{\mathbf{z}}(\mathbf{x}), \sigma_{\mathbf{z}}(\mathbf{x}), \mu_{\mathbf{x}}(\mathbf{z}), \sigma_{\mathbf{x}}(\mathbf{z})) \longrightarrow (\mu_{\mathbf{z}}(\mathbf{x}), \sigma_{\mathbf{z}}(\mathbf{x}), \mu_{\mathbf{x}}(\mathbf{z})) \quad (32)$$

### 822 D.1.4 TRAINING OBJECTIVE MODIFICATION FOR STRONGER CONCENTRATION

823 Inspired by the well known concentration of Gaussian probability measures, to encourage stronger  
824 concentration of the latent code around the spherical shell with radius  $\sqrt{m}$  for better OOD detection,  
825 we propose the following modifications to standard VAEs’ loss functions:

826 We replace the initial KL divergence by:

$$828 \mathcal{D}^{\text{typical}}[Q_{\phi}(\mathbf{z} | \mu_{\mathbf{z}}(\mathbf{x}), \sigma(\mathbf{x})) || P(\mathbf{z})] \quad (33)$$

$$829 = \mathcal{D}^{\text{typical}}[\mathcal{N}(\mu_{\mathbf{z}}(\mathbf{x}), \sigma_{\mathbf{z}}(\mathbf{x})) || \mathcal{N}(0, I)] \quad (34)$$

$$831 = \frac{1}{2} (\text{tr}(\sigma_{\mathbf{z}}(\mathbf{x})) + |(\mu_{\mathbf{z}}(\mathbf{x}))^{\top} (\mu_{\mathbf{z}}(\mathbf{x})) - m| - m - \log \det(\sigma_{\mathbf{z}}(\mathbf{x}))) \quad (35)$$

832 where  $m$  is the latent dimension.

833  
834 In training, we also use Maximum Mean Discrepancy (MMD) Gretton et al. (2012) as a discriminator  
835 since we are not dealing with complex distribution but Gaussian. The MMD is computed with  
836 Gaussian kernel. This extra modification is because the above magnitude regularization does not take  
837 distribution in to account.

838 The final objective:

$$839 \mathbb{E}_{\mathbf{x} \sim P_{\text{ID}}} \mathbb{E}_{\mathbf{z} \sim Q_{\phi}} \mathbb{E}_{\mathbf{n} \sim \mathcal{N}} [\log P_{\theta}(\mathbf{x} | \mathbf{z})] - \mathcal{D}^{\text{typical}}[Q_{\phi}(\mathbf{z} | \mu_{\mathbf{z}}(\mathbf{x}), \sigma(\mathbf{x})) || P(\mathbf{z})] - \text{MMD}(\mathbf{n}, \mu_{\mathbf{z}}(\mathbf{x})) \quad (36)$$

840 The idea is that for  $P_{\text{ID}}$ , we encourage the latent codes to concentrate around the prior’s *typical sets*.  
841 That way,  $P_{\text{OOD}}$  may deviate further from  $P_{\text{ID}}$  in a controllable manner. In experiments, we tried the  
842 combinations of the metric regularizer,  $\mathcal{D}^{\text{typical}}$ , and the distribution regularizer, MMD. This leads to  
843 two other objectives:

$$844 \mathbb{E}_{\mathbf{x} \sim P_{\text{ID}}} \mathbb{E}_{\mathbf{z} \sim Q_{\phi}} [\log P_{\theta}(\mathbf{x} | \mathbf{z})] - \mathcal{D}^{\text{typical}}[Q_{\phi}(\mathbf{z} | \mu_{\mathbf{z}}(\mathbf{x}), \sigma(\mathbf{x})) || P(\mathbf{z})] \quad (37)$$

$$845 \mathbb{E}_{\mathbf{x} \sim P_{\text{ID}}} \mathbb{E}_{\mathbf{z} \sim Q_{\phi}} \mathbb{E}_{\mathbf{n} \sim \mathcal{N}} [\log P_{\theta}(\mathbf{x} | \mathbf{z})] - \mathcal{D}[Q_{\phi}(\mathbf{z} | \mu_{\mathbf{z}}(\mathbf{x}), \sigma(\mathbf{x})) || P(\mathbf{z})] - \text{MMD}(\mathbf{n}, \mu_{\mathbf{z}}(\mathbf{x})) \quad (38)$$

846 where  $\mathcal{D}$  is the standard KL divergence.

847  
848 But we **did not** observe a significant difference in the final AUROC different variations. We still  
849 include those attempted modifications for future work.

## 856 D.2 FEATURE PROCESSING TO BOOST COPOD PERFORMANCES

857  
858 Like most statistical algorithms, COPOD/MD is not scale invariant, and may prefer more dependency  
859 structures closer to the linear ones. When we plot the distributions of  $u(\mathbf{x})$  and  $v(\mathbf{x})$ , we find that  
860 they exhibit extreme skewness. To make COPOD’s statistical estimation easier, we process them by  
861 quantile transform. That is, for ID data, we map the the tuple of statistics’ marginal distributions to  
862  $\mathcal{N}(0, 1)$ . To ease the low dimensional empirical copula, we also de-correlate the joint distribution  
863 of  $(u(\mathbf{x}), v(\mathbf{x}), w(\mathbf{x}))$ . We do so using Kessy et al. (2018)’s de-correlation method, similar to  
Morningstar et al. (2021).



### D.3 WIDTH AND HEIGHT OF A VECTOR INSTEAD OF ITS $l^2$ NORM TO EXTRACT COMPLEMENTARY INFORMATION

In our visual inspection, we find that the distribution of the scalar components of  $(u(\mathbf{x}), v(\mathbf{x}), w(\mathbf{x}))$  can be rather uneven. For example, the visible space reconstruction  $\mathbf{x} - \hat{\mathbf{x}}$  error can be mostly low for many pixels, but very high at certain locations. These information can be washed away by the  $l^2$  norm. Instead, we propose to track both  $l^p$  norm and  $l^q$  norm for small  $p$  and large  $q$ .

**For small  $p$ ,  $l^p$  measures the width of a vector, while  $l^q$  measures the height of a vector for big  $q$ .** To get a sense of how they capture complementary information, we can borrow intuition from  $l^p \approx l^0$ , for small  $p$  and  $l^q \approx l^\infty$ , for large  $q$ .  $\|\mathbf{x}\|_0$  counts the number of nonzero entries, while  $\|\mathbf{x}\|_\infty$  measures the height of  $\mathbf{x}$ . For  $\mathbf{x}$  with continuous values, however,  $l^0$  norm is not useful because it always returns the dimension of  $\mathbf{x}$ , while  $l^\infty$  norm just measures the maximum component.

**Extreme measures help screen extreme data.** We therefore use  $l^p$  norm and  $l^q$  norm as a continuous relaxation to capture this idea:  $l^p$  norm will “count” the number of components in  $\mathbf{x}$  that are unusually small, and  $l^q$  norm “measures” the average height of the few biggest components. These can be more discriminative against OOD than  $l^2$  norm alone, due to the extreme (proxy for OOD) conditions they measure. We observe some minor improvements, detailed in Table 2’s ablation study.

ID: CIFAR10	OOD			
OOD Dataset	SVHN	CIFAR100	Hflip	Vflip
$l^2$ norm	0.96	0.60	<b>0.53</b>	<b>0.61</b>
$(l^p, l^q)$	<b>0.99</b>	<b>0.62</b>	<b>0.53</b>	<b>0.61</b>

Table 2: Comparing the AUC of  $l^2$  norm versus our  $(l^p, l^q)$  measures.

## E ABLATION STUDIES

### E.1 INDIVIDUAL STATISTICS

To empirically validate how  $(u(\mathbf{x}), v(\mathbf{x}), w(\mathbf{x}))$  complement each other, we use individual component alone in first stage and fit the second stage COPOD as usual. We notice significant drops in performances. We fit COPOD on individual statistics  $u(\mathbf{x}), v(\mathbf{x}), w(\mathbf{x})$  and show the results in Table 3. We can see that our original combination in Table 1 is better overall.

### E.2 MD

To test the efficacy of  $(u(\mathbf{x}), v(\mathbf{x}), w(\mathbf{x}))$  without COPOD, we replace COPOD by a popular algorithm in OOD detection, the MD algorithm Lee et al. (2018) and report such scores in Table 1. The scores are comparable to COPOD, suggesting  $(u(\mathbf{x}), v(\mathbf{x}), w(\mathbf{x}))$  is the primary contributor to our performances.

### E.3 LATENT DIMENSIONS

One hypothesis on the relationship between latent code dimension and OOD detection performance is that lowering dimension incentivizes high level semantics learning, and higher level feature learning

Statistic	OOD Dataset			
	SVHN	CIFAR100	Hflip	Vflip
$u(\mathbf{x})$	0.96	0.59	0.54	0.59
$v(\mathbf{x})$	0.94	0.56	0.54	0.59
$w(\mathbf{x})$	0.93	0.58	0.54	0.61
$v(\mathbf{x}) \& w(\mathbf{x})$	0.94	0.58	0.54	0.60
$u(\mathbf{x}) \& v(\mathbf{x})$	0.97	0.61	0.53	0.61
$u(\mathbf{x}) \& w(\mathbf{x})$	0.98	0.61	0.54	0.61

Table 3: COPOD on individual statistics. ID dataset is CIFAR10.

918 can help discriminate OOD v.s. ID. We conducted experiments on the below latent dimensions and  
919 report their AUC based on  $v(\mathbf{x})$  (norm of the latent code) in Table 4  
920

Latent dimension	1	2	5	10	100	1000	3096	5000
$v(\mathbf{x})$ AUC	0.39	0.63	0.52	0.45	0.22	0.65	0.76	0.59

921  
922  
923  
924 Table 4: Lower latent code dimension doesn't help to discriminate in practice.

925  
926 Clearly, lowering the dimension isn't sufficient to increase OOD performances.  
927  
928  
929  
930  
931  
932  
933  
934  
935  
936  
937  
938  
939  
940  
941  
942  
943  
944  
945  
946  
947  
948  
949  
950  
951  
952  
953  
954  
955  
956  
957  
958  
959  
960  
961  
962  
963  
964  
965  
966  
967  
968  
969  
970  
971